Meteorology
and Atmospheric
Physics
Printed in Austria

[1] Department of Aerodynamics, Hellenic Air Force Academy, Dekelia Air Force Base,
 TGA 1010, Dekelia, Attika, Greece
[2] Division of Applied Physics, School of Physics, University of Athens, Athens, Greece

Some considerations on the airborne cloud microphysical probing

Th. I. Lekas[1]**, E. Mavromatidis**[2]**,** and **G. Kallos**[2]

With 11 Figures

Summary

This paper provides a theoretical calibration of Optical Array Probes (OAP) mounted on a given aircraft, in order to take into account the aerodynamic influence of the entire aircraft on the measurements obtained. The measured parameters are corrected through the computation of the air flow-field around the entire aircraft carrying the probes, for different flight conditions, in order to obtain the corresponding undisturbed values. These undisturbed values have been compared to the microphysical ones computed by an atmospheric model, the Regional Atmospheric Modeling System (RAMS). It was found that the removal of the disturbances made by the aircraft on the atmospheric conditions is feasible and provides data that compare much better to the model results. It is suggested that such kind of airborne data corrections may be performed in order to improve the quality of the observations if the aircraft and probe geometries are known. Further information regarding the best location of the OAP probes on the considered aircraft is also obtained.

1. Introduction

Clouds play a critical role on the Earth's climate, the general atmospheric circulation, and the global water balance (Houze RA, Jr, 1993). For this reason, the development of sophisticated cloud parameterizations is needed for more realistic simulations of cloud processes, as well as for providing additional information about other weather phenomena (Kain and Fritsch, 1990; Tremback, 1990; Pielke et al, 1992; Walko et al, 1995; Harrington et al, 1995; Wu, 1999; Jiang and Cotton, 2000; Jiang et al, 2000, 2001 among others). The verification of forecasting systems and algorithms through comparisons to in situ measurements (often airborne), is also a fundamental aspect of the development and improvement process (e.g., Kinne et al, 1992; Guan et al, 2001, 2002; Mavromatidis and Kallos, 2003).

It has been asserted that the passage of an aircraft through a cloud layer for cloud microphysical or air quality observations might result in the production of ice crystals (e.g., Rangno and Hobbs, 1983; Woodley et al, 1991; Kelly and Vali, 1991; Sassen, 1991; Foster and Hallet, 1993). As it has been demonstrated in these works, the ice could be formed by the homogeneous freezing of cloud droplets due to the strong adiabatic expansion and cooling near the propeller tips. Another point is that the measured water content values could also correspond to different upstream values according to the position of the probe on the carrying aircraft. Because of the aerodynamic interference between the probe and

the nearest parts of the aircraft, the trajectories of the atmospheric particles are modified, which in turn modify the measurements.

The purpose of this work is to present a method through which the aerodynamic influence of the entire aircraft on the measurement can be taken into account for given aircraft geometry, flight conditions and probe geometry and location on the aircraft, in order to better approximate the undisturbed cloud microphysics conditions. For this reason, two numerical approaches are adopted. The first is based on the use of the RAMS model, in order to obtain the undisturbed microphysical condition. The RAMS outputs are directly compared with in situ measurements in order to examine the performance of the model. The second, the aerodynamic approach, is based on the flow field computation around the ''Merlin IV'' (see Appendix) aircraft in order to compute Ice Water Content (IWC) at the undisturbed region, based on the measured one. This computation is performed for different locations of the probe on the aircraft, as well as for different angles of attack and aircraft's flight speed. The undisturbed values issued from the two approaches were compared, in order to investigate the influence of the aerodynamic disturbance, caused by the aircraft, on the airborne measurements.

1.1 Case study (the CARL Spring 1999 Experiment)

The measured IWC values used in this paper were obtained during the CARL (Investigation

Table 1. The ranges of particle sizes of the GKSS probes

Instrument	Size range
PMS FSSP-100	2–47 microns
OAP 2D2-C	25–800 microns
OAP 2D2-P	200–6400 microns

of Clouds from ground-based and Airborne Radar and Lidar) program, which was a joint effort between the Institut Pierre Simon Laplace (IPSL/France), GKSS (Germany) and the Atmospheric Modeling and Weather Forecasting Group (AM&WFG) of the University of Athens (Greece). As part of this program, a field campaign took place at the IPSL experimental site in Palaiseau (Paris/France), involving ground-based lidar-radar systems (details can be found in Pelon et al, 2001), as well as airborne measurements (only the latter are used in this paper). The ''Merlin IV'' research aircraft, which flew within the cloud layer by Meteo-France, provided the airborne measurements at different flight levels from 6 to 10 km height. It is a twin-engine turboprop aircraft and in the framework of the project it was carrying the GKSS cloud-particle measuring system (three sizing probes for in-situ microphysical measurements, see Table 1). Data were collected from 26 April to 14 May 1999.

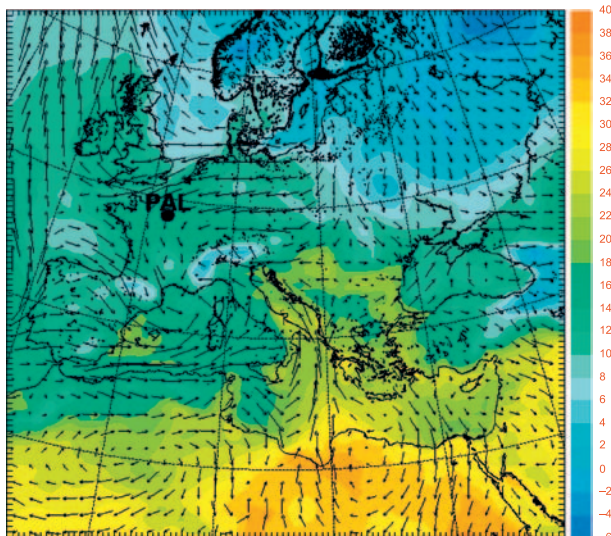## 1.2 Synoptic overview of May 4 cirrostratus/altostratus case

The case chosen for this study consisted of a homogeneous cloud structure (favorable struc-

Fig. 1. ECMWF analysis data, for 12:00 UTC, May 4, 1999: (**a**) Wind field (arrows) and temperature at the first level above the ground (at 2 °C intervals); (**b**) Geopotential height (at 40 m intervals) and temperature (at 2 °C intervals) at the 500 hPa isobaric surface. The location of the experimental site is indicated as PAL (Palaiseau)

Fig. 2. Areas covered by the three nested grids used for the model simulation. The outer grid with 50 km horizontal grid spacing and center at 44° N latitude and 2°15′ E longitude, the second grid with 10 km horizontal grid spacing and center at 48°44′ N latitude and 2°15′ E longitude and the inner grid with 2.5 km horizontal grid spacing and the same center as the second grid. The inner square indicates the center of the 2nd and 3rd grid, which coincides with the coordinates of the experimental site in Palaiseau
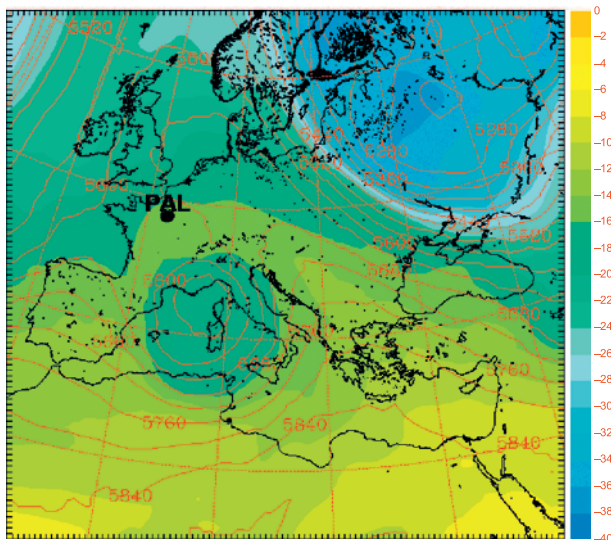
Fig. 3. Time/height cross-section of number concentration of frozen water substances (particles/L multiplied by 0.1). For the preparation of this plot, a vertical column in the model inner domain was extracted from the 3D total ice concentration field, generated by the model simulation, at time intervals of 12 minutes over the grid point that coincides with the position of the experimental site in Palaiseau (Reproduction from Mavromatidis and Kallos, 2003)

Fig. 4. Comparison between aircraft leg-averaged measurements and model averaged values of temperature (°C). The x-axis indicates the constant altitudes of the flight-legs. The model values extracted at the model levels that were the closest to the flight altitude and the averages were calculated over each specific model level

a

temperature [2.0 C]

b

temperature [2.0 C]   geopotential height [40. gpm]

Fig. 1

Fig. 2

Total Ice Concentration [particles/L]

Min value=0.00   [labels *0.1] Max value=46.82
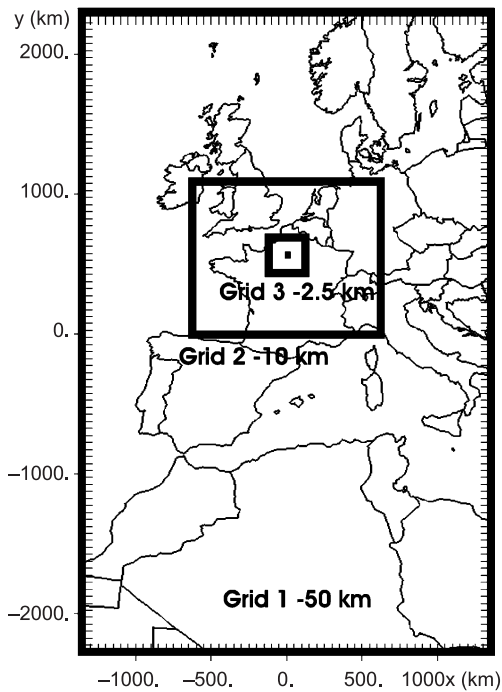
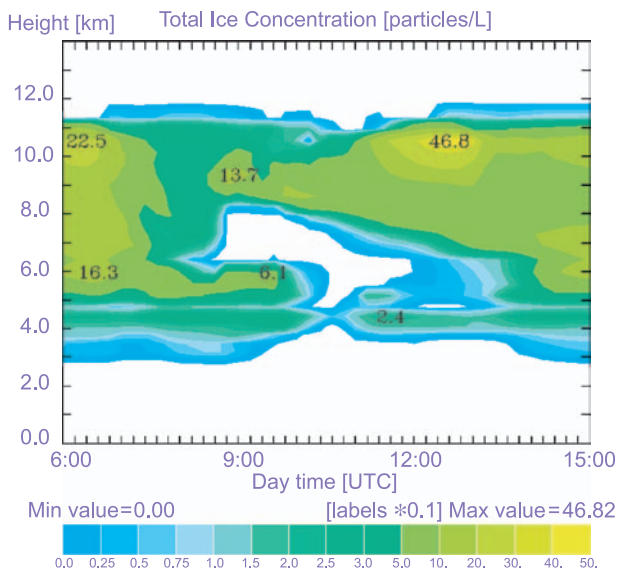**Fig. 3**

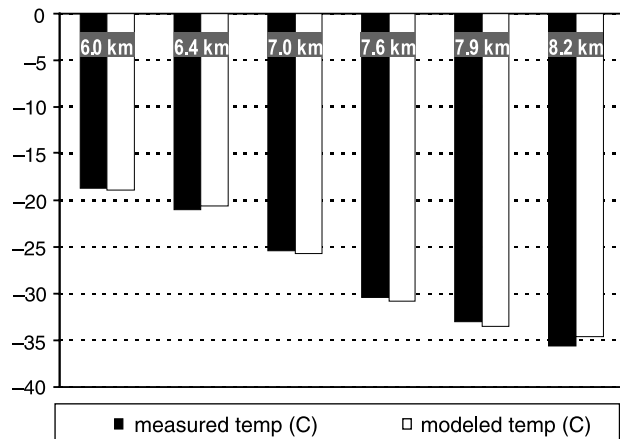■ measured temp (C)   □ modeled temp (C)

Fig. 4

ture for modeling and measurement purposes) observed on the 4 May 1999. On that day, the edge of a frontal cloud field was passing the site (not shown), while a deep low-pressure system located in the middle troposphere moved from the Western Mediterranean over to the Gulf of Genoa. This synoptic pattern caused the transport of continental-type air masses from Eastern Europe towards the lower layers of the atmosphere in the experimental site (Fig. 1a). During the same period strong transport of maritime air masses was evident in the middle and upper troposphere (Fig. 1b). As a result the temperature dropped at the lower atmospheric levels and increased aloft. From early morning the radar detections showed a Ci/Ac cloud, varying in thickness, while a homogeneous and deep Cs/As As cloud formation within the layer 3.5–10.5 km was observed from 09:00 UTC up to about 15:00 UTC (Pelon et al, 2001).

2. Atmospheric modeling approach

2.1 Brief description of the RAMS model

The Regional Atmospheric Modeling System (RAMS) is a well-known numerical code initially developed at Colorado State University and Aster Division of Mission Research Inc. (*http://www. atmet.com*) as a research model (Pielke et al, 1992). The system allows simulations of the atmospheric processes on the scales of a few tens of meters to several thousands of kilometers. Cotton et al (2003) give an overview of the model's current status, focusing on new developments in the RAMS physics and computational algorithms since 1992.

The physical package of the model describes various atmospheric effects, also including the microphysical processes in clouds. The model involves: two-way interactive nested grid structure (Clark and Farley, 1984), terrain following height coordinates, atmospheric turbulent diffusion processes, a modified Kuo cumulus parameterization (Tremback, 1990), cloud radiation schemes (Chen and Cotton, 1983; Harrington, 1997; Harrington et al, 1999), moisture advection and diffusion, a soil-vegetation model (Walko et al, 2000), conversion of water vapor to various types of hydrometeors, various options for upper

and lateral boundary conditions (Klemp and Wilhelmson, 1978; Davies, 1983).

The RAMS version used for the work presented in this paper employs the two-moment scheme for parameterization of cloud microphysics, which introduces ice, liquid and mixed phase hydrometeor categories (Walko et al, 1995; Meyers et al, 1997). This scheme includes prognostic equations for mass mixing ratios of eight forms of water substances, which are: vapor, cloud droplets, rain, pristine ice, snow, aggregates, graupel and hail. Prognostic equations for number concentrations of the same form are also included (except for vapor and cloud droplets).

2.2 Model implementation

For the analysis of the cloud layer, a 48-hour simulation was performed starting at 00:00 UTC 3 May 1999 with a time step of 60 sec. In order to exclude any possible influence on the results of the initial conditions imposed, the model was initialized 24 hours before the day of interest (4 May 1999). The RAMS model was run on three nested grids with a horizontal grid spacing of 50, 10 and 2.5 km (Fig. 2) and used a stretched vertical coordinate (45 levels) for near surface up to 18.3 km. The center of the 2nd and 3rd grid coincides with the location of the experimental site. Vertical nesting has been applied in the second and third grid, permitting adequate resolution of the cloud layer. For these grids (second and third), 51 vertical levels have been used. A summary of the horizontal and vertical grid parameters is provided in Table 2. The physical parameterization schemes used in the model simulation included the microphysics scheme following Walko et al (1995) and Meyers

Table 2. A summary of the grid configuration parameters for all three RAMS grids. The model parameters include the number of grid points in the three directions (nx, ny, nz), the horizontal grid spacing (dx) and the minimum and maximum vertical resolutions (dz min and dz max)

Grids	nx	ny	nz	dx (km)	dz min (m)	dz max (m)
1	55	92	45	50	46	1000
2	122	107	51	10	46	1000
3	94	106	51	2.5	46	1000

et al (1997), the modified Kuo cumulus parameterization scheme (Tremback, 1990), the Chen and Cotton (1983) radiation scheme and an 8-layer soil/vegetation/snow parameterization-LEAF-2 (Walko et al, 2000). The convective parameterization scheme was run on the outer grid, while in all grids the explicit mixed phase microphysics scheme was activated.

The ECMWF (European Center of Medium Range Weather Forecasts) 0.5° gridded objective analysis fields enhanced with soundings and surface observations (retrieved also from the ECMWF) were used for initial and lateral boundary conditions every 6 hours for the whole length of the simulation. An average monthly 1° gridded sea-surface temperature data set (SST) was used for the water body, whereas the topography used for all grids was derived from 30″ resolution terrain data (USGS data set). Finally, gridded vegetation type data (USGS data set) of 30″ resolution was used to derive vegetation cover at each grid cell.

2.3 Results from RAMS simulation

In this section, results of the model-airborne measurements intercomparisons are mainly presented, concerning the fields of temperature, wind speed, wind direction and ice water content (IWC).

Detailed analysis of the cloud microphysical characteristics and dynamics based on the model results of the same case study is reported in Mavromatidis and Kallos (2003). As it is mentioned in this work, a strong wind shear over the experimental site could be responsible for cloud formation in the vertical during the initial stages of the cloud development. The maximum wind speed reached 15.75 m/s at the cloud base (∼3.5 km) and 26.35 m/s at the cloud top (∼10 km), while wind direction changed with altitude from 40° up to 180°. The zero degree isotherm was located at about 2.8 km ASL in agreement to the height obtained from a sounding close to the experimental site. The vertical component of the wind (w) was characterized by velocities in a range from −0.14 to 0.26 m/s, which are typical values for similar cloud systems. The model simulation showed that the lower levels of the cloud deck (the layer between 3–5 km) were characterized by concentration of

Table 3. Leg-Averaged Values of Wind Speed and Direction ("Data" Columns) and Averaged Values of the Model Results ("Model" Columns) at altitudes that were the closest to the flight levels. Column 1 indicates the flight altitudes and column 2 indicates the altitude of the considered model levels

Leg [Z(km)]	Model levels	Wind speed (m/s)		Wind direction (deg)	
		Model	Data	Model	Data
1 (6.0)	6.0 km	5.43	6.03	128	131
2 (6.4)	6.5 km	4.41	5.69	134	150
3 (7.0)	6.9 km	4.71	7.54	131	143
4 (7.6)	7.5 km	6.90	8.35	138	150
5 (7.9)	7.9 km	8.55	7.78	138	162
6 (8.2)	8.3 km	9.32	8.18	145	165

aggregates, while snow particles dominated at levels above the height of 5 km. Pristine ice particles of small diameter and low density prevailed throughout the cloud body with the highest concentrations at the cloud top (∼10 km). The cloud boundaries, as well as the variation of the total ice concentration over the experimental site for a 9-hour period are shown in Fig. 3.

Initially, for direct comparisons with observations, leg-averaged measurements (approximately 400-s time intervals) were compared with averaged values of model results for three meteorological fields, namely, temperature, wind speed and direction. The aircraft collected the data between 11:00 and 14:00 UTC over an area around the experimental site during six constant-altitude flight legs (see Table 3), while the model values were extracted at the model levels that were the closest to the flight altitudes and the averages were calculated at each specific model level (Table 3).

It should be pointed out that the in situ aircraft measurements are based on samples of only a few m^3 as compared to the model grid volume, which are of approximately 10^{11} m^3. Despite this, airborne observations are the only existing source of direct cloud microphysical measurements, which allow for direct comparison to the results of atmospheric models. However, the simulated temperature compares well to the observed temperature during the aircraft measurements (Fig. 4). Consistent with the aircraft observations were also the wind speed and direction (Fig. 5 and Table 3). More specifically, the model slightly underestimated the wind speed at lower altitudes,
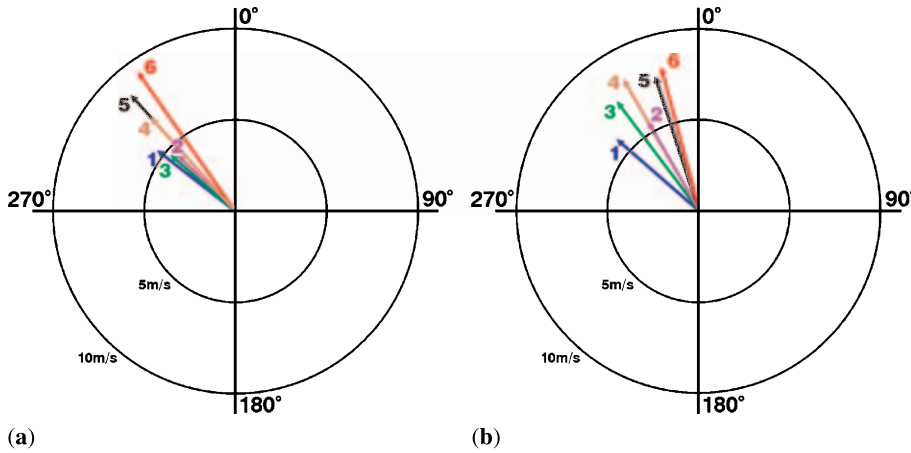
Fig. 5a. Modeled wind speed and direction at the considered model levels (shown in Table 3), and (**b**) measured wind speed and direction at the considered flight levels (shown in Table 3). All wind speed arrows are shown at the same scale. Wind vectors for the same level are denoted by the same number and color

while this field was slightly overpredicted at upper levels. An exception was observed for the third flight leg (7 km), where more serious differences were found. Within this flight altitude the simulated wind speed was significantly lower (37%) than the measurements. Wind direction differences are within a range of less than twenty five degrees throughout the entire layer where measurements were taken.

On the second stage, the measured data were analyzed over 50-s averaging intervals for every flight leg over distinct, 2.5-km grid points, within the model's inner domain (grid 3 in Fig. 2), coinciding with the area covered by the "Merlin IV" flights. The modeled data was extracted from the 3D-fields over these specific grid points at model levels close to the altitudes of the flight legs.

To gain insight into the accuracy of the cloud microphysical simulations, comparisons between the model and aircraft IWC were made. A scatter plot of model and measured IWC is displayed in Fig. 6 with the square of the corresponding linear correlation coefficient. As it is shown, the simulated IWC values compare quite well with those derived from the measurements. It should be noted that the comparisons shown in this work are for ice particles with diameters greater than 25 microns. This is because the modeled IWC and number concentration for small size particles (diameter < 25 microns) deviate significantly from the measurements, with the model values being highly underpredicted (approximately three orders of magnitude). This deviation may be attributed to the reduced accuracy of the measuring system or to the model parameterization or both.
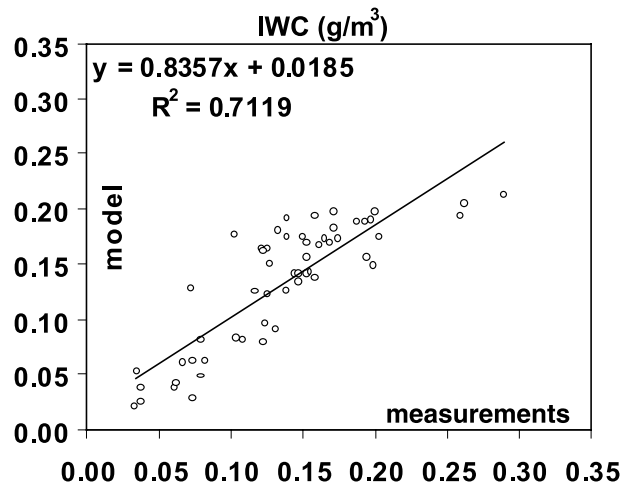

Fig. 6. RAMS simulated IWC versus measured values for all flight-legs. The model values are extracted at the model levels that were the closest to the flight altitudes. The solid curve represents the least square regression line. The least square regression line equation and the square of the linear correlation coefficient (R^2) are also shown

More specifically, in the present work the characteristics of small size ice particles were measured by an FSSP-100 probe (see Table 1). The FSSP is designed to measure droplet characteristics although it responds significantly to ice particles. Details and uncertainties related to the FSSP measurements can be found in Baumgardner et al (1985) as well as in Gardiner and Hallet (1985), who examined the splintering of ice particles on the front of a FSSP. They showed that, because of the generation of many small ice particles due to the splintering, false counts due to ice particles could be as high as two or three orders of magnitude greater than the

actual ice crystal number concentration. As far as the RAMS simulation is concerned, it seems that the microphysical scheme fails to correctly generate small sized ice particles, which needs further investigation.

As such, the comparison of modeled and observed values on the small size particles cannot be considered as complete and it is not further discussed in this paper.

3. Modeling approach through aircraft aerodynamics

The atmospheric particles have mass and therefore inertia, which determines how closely they will follow the streamlines. The higher the inertia, the higher the difference between the local flow velocity and the particle velocity. This velocity difference makes that a fluid force is exerted on the particle. The higher the value of the fluid force, the higher the deviation of the particle trajectory from the streamlines, especially at regions of high curvature. In this section, a numerical approach is presented in order to handle this problem.

A trajectories tube from the undisturbed region (starting plane) to the probe (target plane) is shown in Fig. 7. Assuming that, for a given atmospheric particles class the trajectories have no common point, there is a water mass conservation through the trajectories tube. This leads to the following equation:
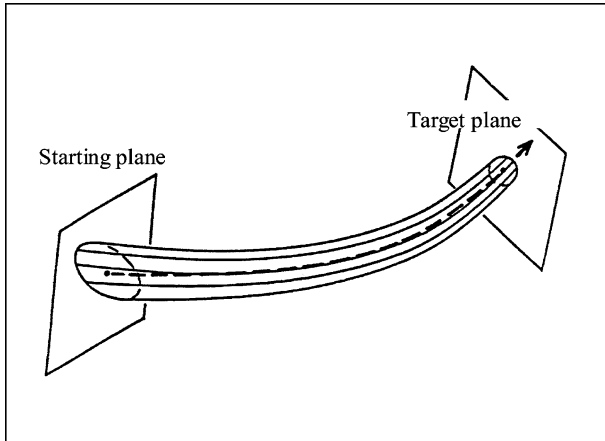
$$W_\infty S_\infty V_\infty = W_T S_T V_T, \tag{1}$$

Fig. 7. Trajectories tube

where the indices T and ∞ are referred to the near probe (target) regions and the undisturbed respectively while W, S and V are the IWC or LWC (g/m^3), starting and target area (m^2) and particle velocity far and close to the probe, respectively. The quantity, which must be determined, is W_∞ (undisturbed IWC or LWC). From Eq. (1) it follows that:

$$W_\infty = \frac{W_T S_T V_T}{S_\infty V_\infty}. \tag{2}$$

In Eq. (2), the following quantities are known:

V_∞ = flight speed (TAS: true air speed),
W_T = measured LWC or IWC,
S_T = probe frontal area,

S_∞ and V_T must be calculated and in order to do this a particle trajectory computation is needed. The contour of S_T is approximated by a number of (known) points. Same procedure for S_∞ but in this case the points of this contour must be determined. Each point of S_∞ contour (starting point) corresponds to a point of S_T contour (target point).

This computation, which is a Lagrangian approach, starts with a first estimation of the starting point, which corresponds to a given target. Then, the trajectory is computed by solving step by step the equation of motion of the particle. The calculation stops when the target area is reached and after a correction of the starting point position is repeated until the final point of the trajectory and the target point are as close as the user prescribes. Once the final point of the trajectory is known, V_T is also known.

The particle equation of motion is

$$m_P \frac{d\vec{V}_P}{dt} = \vec{F}_{AER} + \vec{F}_B + \vec{F}_A + \vec{F}_I + \vec{F}_O$$
$$+ \vec{F}_{OR} + \vec{W}_P, \tag{3}$$

where:

m_P = particle mass
$\vec{V}_P$ = particle velocity at any point of its trajectory
$\vec{F}_{AER}$ = aerodynamic force
$\vec{F}_B$ = Basset force (depends on the history of the particles motion)
$\vec{F}_A$ = Archimedes force
$\vec{F}_I$ = force due to the inertia of the displaced fluid (by the particle)

$\vec{F}_O$ = force due to the existence of a transversal velocity gradient regarding to the particle direction of motion

$\vec{F}_{OR}$ = force due to the attitude of the particle regarding to the local flow direction

$\vec{W}_P$ = particle weight.

A first estimation shows that, all forces are negligible, compared to $\vec{F}_{AER}$ and $\vec{W}_P$ (Guffond, 1981). $\vec{F}_{AER}$ is due to the particle inertia, which forces the particle to move slower than the local flow and its module is

$$\vec{F}_{AER} = \frac{1}{2}\rho_{AIR}S_P C_D(\vec{V}_f - \vec{V}_P)^2, \qquad (4)$$

where:

ρ_{AIR} = air density at the considered flight level

S_P = particle frontal area

C_D = particle drag coefficient (depends on the particle habit)

$\vec{V}_f$ = local flow velocity.

The particle drag coefficient is calculated as a function of the Reynolds number and of the habit of the particle (Clift et al, 1978; Beard, 1976; Auer and Veal, 1970). It is also assumed that the particle can respond spontaneously to any local flow direction change, so its frontal surface is always normal to the local flow direction.

According to the above, the particle equation of motion is

$$m_p\frac{d\vec{V}_p}{dt} = \frac{1}{2}\rho_{AIR}S_P C_D \frac{(\vec{V}_f - \vec{V}_p)}{|\vec{V}_f - \vec{V}_p|}|\vec{V}_f - \vec{V}_p|^2 + \vec{W}_p, \qquad (5)$$

which is solved step-by-step using a 4th-order Runge-Kutta scheme. The dependence of Eq. (5) on the local flow velocity V_f requires that the flow characteristics at any point around the probe (so around the aircraft) must be known.

In order to compute the flow field characteristics at any point around the aircraft, an in-house vortex lattices panel method code was used (Katz and Plotkin, 1991). This choice was driven by the need for fast obtainable accurate results. This approach is also not demanding as far as computer memory is concerned. The code has been used in the past for several applications and types of aircrafts either civil or military.

3.1 Calculation of the flow field around the entire aircraft including probes

3.1.1 Position of the problem

The aerodynamic flow field around the aircraft must be known as a function of the aircraft's geometry, flight speed, attitude (angle of attack), and sideslip angle. It should be noted that in the aircraft's geometry the shape of the probes, as well as their exact location on the aircraft are also included.

Due to the complex geometry involved, only a numerical approach is possible. There are well known numerical approaches where the air is considered either as a viscous or a non-viscous fluid, but in any case the geometry must be described by points combined in order to form elementary surfaces, which approximate the surface of the aircraft. Depending on the approach, the flow field parameters are computed for given flight conditions using Navier-Stokes equations (viscous approach), Euler equations or a Singularities method (non-viscous approach).

In the case of Navier-Stokes and Euler equations a grid must be generated on and around the aircraft at each node of which the flow parameters are computed. This approach demands high memory capacity, it is time consuming and it is not always converging. On the other hand, there is no need for grid around the aircraft in the case of Singularities method. This approach is not very demanding in memory capacity and is generally fast converging. For this reason it was adopted in our case.

3.1.2 Singularities method (Panel method)

The local flow velocity at any point around the aircraft (or around an immersed obstacle in a moving fluid in general) is the vector sum of two other velocities: the free stream (undisturbed) velocity, which would be observed at the considered point in the absence of the obstacle and the disturbance velocity, which is due to the presence of the obstacle. In our case the free stream velocity is known (flight speed), so if the disturbance velocity is computed, the local flow velocity can be defined.

In order to compute the disturbance velocity at any point of the flow field, singularities of unknown strength are considered on any elementary surface (panel) used to approximate the air-

craft's geometry. Different types of singularities can be used, such as sources, doublets or vortex lattices. The strength of those singularities is different from an elementary surface to another. A Neumann type boundary condition is applied at any point of the surface of the aircraft (usually the centroid of every elementary surface), which states that the vector sum $\vec{V}_R$ of the free stream velocity $\vec{V}_R$ (flight speed) and of the local disturbance velocity $\vec{V}_{DIST}$ must be tangent to the surface at the point considered. This is a slip condition and physically means that the surface of the obstacle is considered as a stream surface because, as it was mentioned earlier, the air is considered as a non-viscous fluid. The mathematical translation of this boundary condition is that the scalar product of the local velocity $\vec{V}_R$ by the local external normal unit vector of the surface $\vec{n}$ equals to zero.

$$\vec{V}_R \cdot \vec{n} = 0. \tag{6}$$

The local disturbance velocity is the vector sum of the velocities induced by the singularities of every elementary surface on the considered point (so it is a function of their strength).

The velocity induced by a singularity located at the panel j at the centroid of the panel i depends on the strength of this singularity, on its distance from the targeted centroid and on the exact shape of the panel carrying the singularity. As the geometry of the aircraft is known the induced velocity can be considered as the product of a velocity induced by a singularity of unit strength (which can be calculated) times the actual strength of the singularity, which is unknown. In this way, the disturbance velocity at the centroid i induced by the singularities of every panel approximating the surface of the aircraft (including i) is

$$\vec{V}_{DISTi} = \sum_{j=1}^{N} \vec{v}_{ij}\sigma_j, \tag{7}$$

where, $\vec{v}_{ij}$ is the velocity induced by a singularity of unit strength located at the panel j on the centroid of the panel i, σ_j is the unknown strength of the singularity located at the panel j and N is the total number of panels, which approximate the surface of the aircraft. It must be noted here that the velocity induced by the singularity of the targeted panel (panel i) on its own centroid is also taken into account (self-induction).

Equations (6) and (7) applied to the centroid of panel i, are giving:

$$(\vec{V}_\infty + \vec{V}_{DISTi}) \cdot \vec{n}_i = 0 \Rightarrow \vec{V}_{DISTi} \cdot \vec{n}_i$$

$$= -\vec{V}_\infty \cdot \vec{n}_i \Rightarrow \sum_{j=1}^{N} \vec{v}_{ij}\sigma_j \vec{n}_i$$

$$= -\vec{V}_\infty \cdot \vec{n}_i \Rightarrow \sum_{j=1}^{N} A_{ij}\sigma_j$$

$$= -\vec{V}_\infty \cdot \vec{n}_i, \tag{8}$$

where A_{ij} is the scalar product of $\vec{v}_{ij}$ and $\vec{n}_i$ (both quantities are known because the geometry of the aircraft is known). If the same boundary condition is applied at the centroid of every panel (i.e., N centroids), a system of $N \times N$ linear algebraic equations is formed with N unknowns, which are the strengths of the singularities. Once the strengths are known, using the mathematical expression corresponding to the used type of singularity the flow velocity vector at any point of the flow field can be computed.

In any case the mathematical expression giving the induced velocity by the singularity at a given point is different according to the type of singularity, but the approach described above remains the same. In our case the singularities used were vortex lattices, while their induced velocity vector is given by the Biot-Savart law.

3.2 Results from the aerodynamic approach and discussion

The purpose of the simulations was to investigate the influence on the accuracy of the measurements, of the location of the probe on the aircraft, for various flight conditions. The computation is performed for different locations of the probe on the aircraft, as well as for different angles of attack and aircraft's flight speed, while the IWC values measured by the "Merlin IV" were used as input. The geometry of the aircraft and the probe is taken into account. Then, the obtained undisturbed values were compared to those issued from the RAMS model.

A numerical model of the aircraft and the probe was made, on an in-house pre-processor, coupled with the aerodynamic code. The aircraft's basic geometry was found in Jane's World Aircrafts.

Several runs of the aerodynamic code were performed in order to determine the lift coefficient versus the angle of attack curve of the aircraft. This curve was compared to the one obtained, using approximate method (Torenbeek, 1999) in order to check the flow field computation. The flow field around the aircraft and the probe was computed for two different angles of attack (AOA) corresponding to two different flight speeds but in such a way that the lift was kept constant. This was done in order to examine the influence of the aircraft attitude (angle of attack) on the measured IWC.

Similar approaches were used by King (1985), Norment (1980), and Norment and Zalosh (1974) among others. The codes used by the above mentioned authors were source-sink panel based and the flow field around the fuselage was mainly concerned, while in this study the flow field around the entire aircraft, including the probes, is investigated.

As it is discussed in Sect. 2.3 and was presented in detail in Mavromatidis and Kallos (2003), the RAMS model had accurately predicted the characteristics (e.g., the spatial and temporal variability of the phenomena and the cloud geometry) as well as the conditions leading to the formation of the cloud system under study. It should be pointed out that the IWC measurements of "Merlin IV" were taken with a probe

located at the nose of the aircraft. At 6 km of flight altitude a good agreement was found between the measured and simulated by the RAMS IWC values (Fig. 8). For this reason, RAMS outputs are taken to be the undisturbed conditions (reference conditions) at this flight level and the obtained undisturbed values (from the aerodynamic approach) were compared to those resulted from the RAMS. In all cases the procedure followed was the same, hence the results from 6 km constant flight level (leg 1 in Table 3) presented here are considered as representative. The habit of the encountered particles is determined as a function of the flight level temperature and was found, according to Pruppacher and Klett (1997), to be a combination of bullets (specified as c2a by the above authors).

Figure 9 shows the IWC computed with RAMS versus the undisturbed IWC values (which are calculated from the aerodynamic approach and based on the measured IWC) for two different attitudes and flight speeds for a probe that is located under the wing. The probe for this approach is placed at 40 cm from the lower wing surface. The higher the aircraft's angle of attack (AOA), the higher the measurement distortion introduced.

Similar results to Fig. 9 are shown in Fig. 10, but in this case the probe was located either at the nose region of the aircraft or under the wing. In the case of the under the wing position the probe was located either at 40 cm or at 60 cm under the lower wing surface. As it is shown, when the probe is located at 40 cm from the lower wing surface an average measurement distortion of about 28% is introduced relatively to the case when the probe is located at 60 cm from the lower wing surface. In both cases the spanwise and chordwise location of the probe is the same. The measurement distortion decreases as the distance of the probe from the lower wing surface is increased. This is due to the local flow distortion, which influences the particle trajectories. It can be assumed that if the probe was not completely under the wing, due to local flow distortion, the differences between measured and calculated IWC would be more important when the front of the probe is located close to the leading edge of the wing. The case for which the probe is located at the nose is shown in Fig. 11. It can be seen that the nose position has very little influence on the measurements as expected due to the local flow.
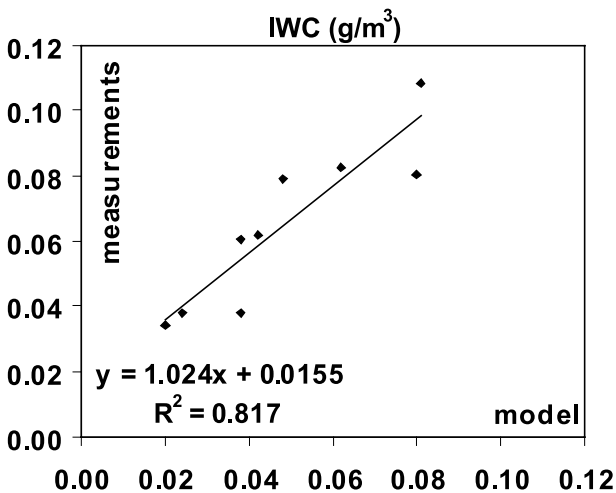

Fig. 8. RAMS simulated IWC versus measured values for the first flight leg (6 km constant flight level). The model values are extracted at the model level that was the closest to the flight altitude. The solid curve represents the least square regression line. The least square regression line equation and the square of the linear correlation coefficient (R^2) are also shown

The smaller trajectories' distortion corresponds to flights at 0 degrees of attitude, which was expected due to the smaller flow distortion in this case. From these figures, it can be also seen that in order to compare airborne measurements at a different probe location on the aircraft, the flight speed and attitude must be the same for a given aircraft configuration. In the present study the probe was located at the nose of the aircraft.
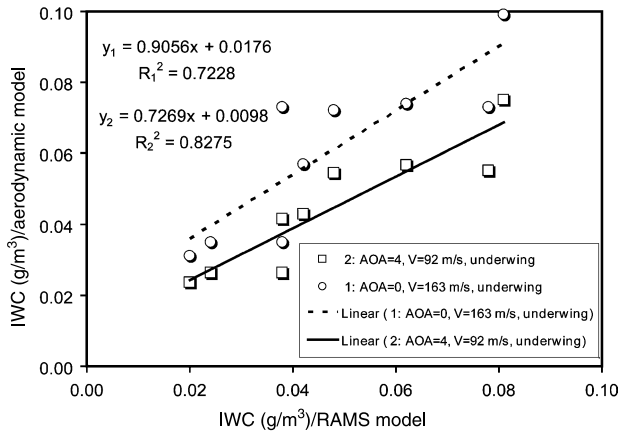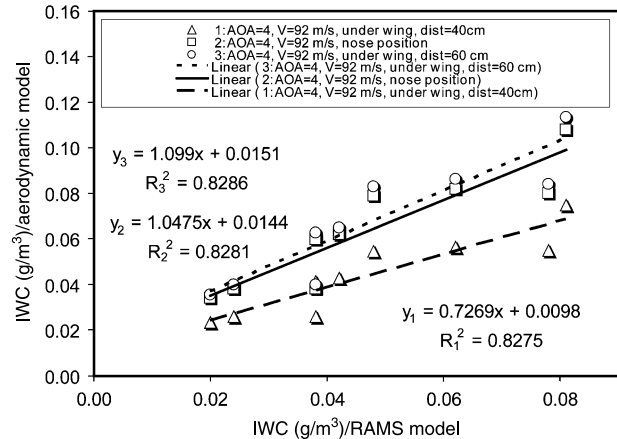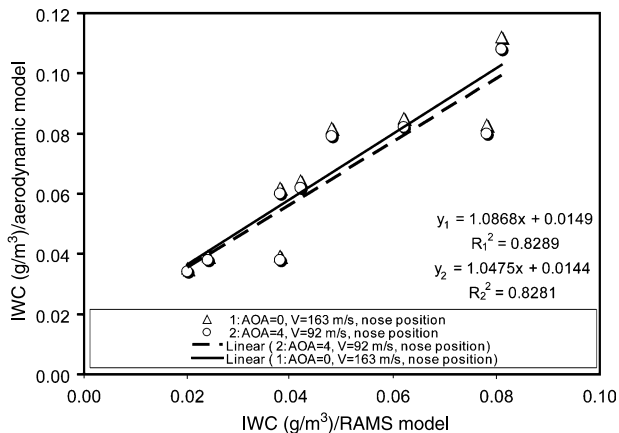

Fig. 9

Fig. 10

Fig. 11

Fig. 9. IWC computed with RAMS versus the undisturbed IWC values (which are calculated from the aerodynamic approach and based on the measured IWC) for a probe that is located under the wing. Two different flight conditions (V: flight speed and AOA: angle of attack) were considered. The diameters of ice crystals were taken equal to 104 microns. The solid curves represent the least square regression line for each case. The least square regression line equations and the correlation coefficients (R^2) are also shown

Fig. 10. IWC computed with RAMS versus the undisturbed IWC values (which are calculated from the aerodynamic approach and based on the measured IWC) for same flight conditions and for two different probe locations: under the wing (two distances from the wing) and nose. The diameters of ice crystals were taken equal to 104 microns. The solid curves represent the least square regression line for each case. The least square regression line equations and the correlation coefficients (R^2) are also shown

Fig. 11. IWC computed with RAMS versus the undisturbed IWC values (which are calculated from the aerodynamic approach and based on the measured IWC) for a probe that is located under the nose. Two different flight conditions were considered: (**a**) flight speed (V) equal to 163 m/s and angle of attack (AOA) equal to 0 degrees, and (**b**) flight speed (V) equal to 92 m/s and angle of attack (AOA) equal to 4 degrees. The diameters of ice crystals were taken equal to 104 microns. The solid curves represent the least square regression line for each case. The least square regression line equations and the correlation coefficients (R^2) are also shown

4. Conclusions

In this work an attempt was made to propose a methodology for highlighting some inaccuracies involved in airborne measurements (cloud microphysics) due to the presence of the aircraft, the flight conditions and the location of the probes on the aircraft. This methodology could be used to regularize various airborne measurements for a given aircraft configuration.

In a first stage, cloud and microphysics simulations performed with the RAMS model were compared with in situ aircraft measurements. These comparisons were made to investigate the performance of the model in the context of the specific case study. The aircraft data were collected during 6 flights from a research field program and were averaged over a 50-s time interval (approximately 2.5 km of horizontal distance in x-direction) for comparison with the model grid data.

In general, the model succeeded in producing the cloud with the geometrical thickness observed and at the right location. A quantitative comparison of the simulated and observed temperature field showed high linear correlation. The verification results for the wind field showed an overestimation of the simulated wind speed at the upper flight levels, while it was under-predicted at the lower altitudes. The comparisons between the model and measured IWC showed poor model performance for the small size frozen water substances (diameters smaller than 25 microns). On the contrary, the modeled IWC (for diameters greater than 25 microns) compares quite well to the observations. The linear correlation was almost 0.85:1, without excessive dispersion.

The undisturbed IWC of a cloud was computed based on its measured value. This approach consists in the flow computation around the entire aircraft which carries the probes, including the probes, followed by an atmospheric particle trajectories calculation.

It was found that the probe location on the aircraft as well as the flight conditions lead to different undisturbed IWC values for a given measured IWC data set. This suggests that in order to compare different airborne measurements, it is important that the above parameters are to be kept constant for a given aircraft configuration. This also means that the probe location on the aircraft must be chosen in such a way that the local flow disturbance is minimal.

Appendix

Fairchild "Merlin IV" aircraft characteristics (from Meteo France-www.cnrm.meteo.fr)

Max. endurance	3 up to 5 h (with IFR reserves)
Max. range	2.200 km at 8.000 m alt. (1200 NM)
Initial climb	22.000 ft (6.700 m)
Max. altitude	24.500 ft (7550 m)
Min. altitude	Over water:200 ft (62 m) for 60 Nm or 500 ft(155 m) during 15 minutes Over land: 150 ft(46) for 60 Nm or 500 ft(155 m) during 15 minutes
Speed	75–135 m/s
Max. payload	500 kg
Crew	2 aircrew + 1 technician up to 2 scientists

References

Auer AH Jr, Veal DL (1970) The dimension of ice crystals in natural clouds. J Atmos Sci 27: 919–926

Baumgardner D, Strapp JW, Dye JE (1985) Evaluation of the forward scattering spectrometer probe. II: Corrections for coincidence and dead-time losses. J Atmos Oceanic Technol 2: 626–632

Beard KV (1976) Terminal velocity and shape of cloud precipitation drops aloft. J Atmos Sci 33: 851–864

Chen C, Cotton WR (1983) A one-dimensional simulation of the stratocumulus-capped mixed layer. Bound Layer Meteorol 25: 289–321

Clark TL, Farley RD (1984) Severe downslope windstorm calculations in two and three spatial dimensions using anelastic interactive grid nesting: A possible mechanism for gustiness. J Atmos Sci 41: 329–350

Clift R, Grace JR, Weber ME (1978) Bubbles, drops and particles. New York: Academic Press

Cotton WR, Pielke RA Sr, Walko RL, Liston GE, Tremback CJ, Jiang H, McAnelly RL, Harrington JY, Nicholls ME, Carrio GG, McFadden JP (2003) RAMS 2001: Current status and future directions. Meteorol Atmos Phys 82: 5–29

Davies HC (1983) Limitations of some common lateral boundary schemes used in regional NWP models. Mon Wea Rev 111: 1002–1012

Foster TC, Hallett J (1993) Ice crystals produced by expansion: experiments and application to aircraft-produced ice. J Appl Meteor 32(4): 716–728

Gardiner BA, Hallett J (1985) Degradation of in-cloud forward scattering spectrometer probe measurements in the presence of ice particles. J Atmos Oceanic Technol 2: 171–180

Guan H, Cober SG, Isaak GA (2001) Verification of super-cooled water forecasts with in situ aircraft measurements. Wea Forecast 17: 1226–1235

Guan H, Cober SG, Isaak GA, Tremblay A, Methot A (2002) Comparison of three cloud forecast schemes with in situ aircraft measurements. Wea Forecast 16: 145–155

Guffond D (1981) Ice accretion on a protected surface during a flight in icing conditions (in French). ONERA, RT, No 3/5146 SY

Harrington JY (1997) The effects of radiative and microphysical processes on simulated warm and transition season Arctic stratus. PhD Diss. Atmospheric Science Paper No 637, Colorado State University, Department of Atmospheric Science, Fort Collins, CO 80523, 289 pp

Harrington JL, Cotton WR, Meyers MP, Walko RL (1995) Parameterization of ice crystal conversion processes due to vapor deposition for mesoscale model using double-moment basis functions. Part I: Basic formulation and parcel model results. J Atmos Sci 52: 4344–4366

Harrington JY, Reisin T, Cotton WR, Kreidenweis SM (1999) Cloud resolving simulations of Arctic stratus. Part II: Transition-season clouds. Atmos Res 55: 45–75

Houze RA Jr (1993) Cloud dynamics. International Geophysical Series, Vol. 53, New York: Academic Press

Jane's world aircraft, 1999–2000 (edited by Paul Jackson) MRAeS

Jiang H, Cotton WR (2000) Large-eddy simulation of shallow cumulus convection during BOMEX: Sensitivity to microphysics and radiation. J Atmos Sci 57: 582–594

Jiang H, Cotton WR, Pinto JO, Curry JA, Weissbluth MJ (2000) Cloud resolving simulations of mixed-phase Arctic stratus observed during BASE: Sensitivity to concentration of ice crystals and large-scale heat and moisture advection. J Atmos Sci 57: 2105–2117

Jiang H, Feingold G, Cotton WR, Duynkerke PG (2001) Large-eddy simulations of entrainment of cloud condensation nuclei into the Arctic boundary layer: 18 May, 1998 FIRE/SHEBA case study. J Geophys Res 106: 15 113–15 122

Kain JS, Fritsch JM (1990) A one-dimensional entraining/detraining plume model and its application in convective parameterization. J Atmos Sci 47, 23, 2784–2802

Katz J, Plotkin A (1991) Low speed aerodynamics. Mc Graw-Hill

Kelly RD, Vali G (1991) An experimental study of the production of ice crystals by a twin-turboprop aircraft. J Appl Meteor 30(2): 217–226

King WD (1985) Air flow and particle trajectories around aircraft fuselages. Part III: extensions to particles of arbitrary shape. J.A.O.T., pp 539–547

Kinne S, Ackerman TP, Heymsfield AJ, Valero FPJ, Sassen K, Spinhirne JD (1992) Cirrus microphysics and radiative transfer: cloud field study on 28 October 1986. Mon Wea Rev 120(5): 661–684

Klemp JB, Wilhelmson RB (1978) The simulation of three-dimensional convective storm dynamics. J Atmos Sci 35: 1070–1096

Mavromatidis E, Kallos G (2003) An investigation of cold cloud formation with a three-dimensional model with explicit microphysics. J Geophys Res 108(D14): 4420–4441

Mellor GL, Yamada T (1982) Development of a turbulence closure model for geophysical fluid problems. Rev Geophys Space Phys 20: 851–875

Meyers MP, Walko RL, Harrington JY, Cotton WR (1997) New RAMS cloud microphysics parameterization. Part II: the two-moment scheme. Atmos Res 45: 3–39

Norment HG (1980) Calculation of water drop trajectories to and about arbitrary three-dimensional bodies in potential air flow. NASA contractor report 3291

Norment HG, Zalosh RG (1974) Effects of airplane flow field on hydrometeor concentration measurements. Report, Air Force Cambridge Research Laboratories. TR-74-062

Pelon J, Testud J, Noel V, Tinel C, Guyot A, Caillaud K, Protat A, Chepfer H, Trouillet V, Baudin F, Flamant H, Quante M, Nagel D, Lemke H, Danne O, Albers F, Raschke E, Kallos G, Mavromatidis E (2001) Investigation of Cloud by Ground-based and Airborne Radar and Lidar (CARL). Final Report for the European Commission, DGXII, Contract PL-970567

Pielke RA, Cotton ER, Walko RL, Tremback CJ, Lyons WA, Grasso LD, Nicholls ME, Moran MD, Wesley DA, Lee TJ, Copeland JH (1992) A comprehensive meteorological modeling system – RAMS. Meteorol Atmos Phys 49: 69–91

Pruppacher RH, Klett JD (1997) Microphysics of clouds and precipitation, 2nd revised and enlarged edition. Kluwer Academic Publishers. Atmospheric and Oceanographic Sciences Library, Vol. 18

Rangno AL, Hobbs PV (1983) Production of ice particles in clouds due to aircraft penetration. J Climate Appl Meteor 22: 214–232

Sassen K (1991) Aircraft-produced ice particles in a highly supercooled altocumulus cloud. J Appl Meteor 30(6): 765–775

Torenbeek E (1999) Synthesis of subsonic airplane design. Delft University Press Kluwer Academic Publishers

Tremback CJ (1990) Numerical simulation of a mesoscale convective complex: model development and numerical results. Ph.D. Dissertation, Atmos Sci Paper No. 465, Colorado State University, Dept. of Atmospheric Science, Fort Collins, CO 80523

Walko RL, Cotton WR, Meyers MP, Harrington JY (1995) New RAMS cloud microphysics parameterization. Part I: the single moment scheme. Atmos Res 38: 29–62

Walko RL, Band LA, Baron J, Kittel TGF, Lammers R, Lee TJ, Pielke RA Sr, Taylor Ch, Tague Ch, Tremback CJ, Vidale PL (2000) Coupled atmosphere-biophysics-hydrology models for enviromental modelling. J Appl Meteorol 39(6): 931–944

Woodley WL, Henderson TL, Vonnegut B, Gordon G, Breidenthal R, Holle SM (1991) Aircraft-produced ice particles (APIPs) in supercooled clouds and the probable mechanism for their production. J Appl Meteor 30(11): 1469–1489

Wu T (1999) Numerical modeling study of the November 26, 1991 cirrus event. PhD Diss., Colorado State University, Department of Atmospheric Science, Fort Collins, CO 80523, 188 pp

Corresponding author's address: Kallos George, University of Athens, School of Physics, Division of Applied Physics, University Campus, Bldg PHYS-V (E-mail: kallos@mg.uoa.gr)